Title

A Comprehensive Analysis of the Variably Saturated Hydraulic Behavior of a Green Roof in a Mediterranean Climate

Journal

Vadose Zone Journal, 15(9)

ISSN

1539-1663

Authors

Brunetti, Giuseppe
Šimůnek, Jirka
Piro, Patrizia

Publication Date

2016-09-01

DOI

10.2136/vzj2016.04.0032

Peer reviewed

Published August 25, 2016

Original Research

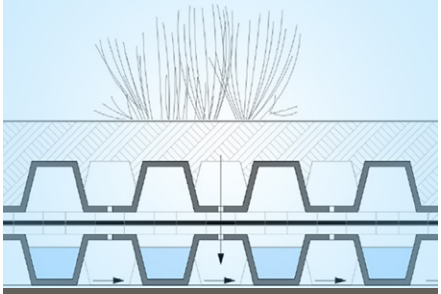

A Comprehensive Analysis of the Variably Saturated Hydraulic Behavior of a Green Roof in a Mediterranean Climate

Giuseppe Brunetti,* Jirka Šimůnek, and Patrizia Piro

Low-impact developments (LIDs), such as green roofs, have proven to be valuable alternatives for stormwater management and hydrological restoration. Mechanistic models are reliable and accurate tools for analysis of the hydrologic behavior of LIDs, yet only a few studies provide a comprehensive numerical analysis of the hydrological processes involved and test their model predictions against field-scale data. Moreover, more research is needed to determine the unsaturated hydraulic properties of the substrates used in LIDs. For these reasons, the aim of this study was to provide a comprehensive description of the hydrological behavior of an extensive green roof installed at the University of Calabria. The soil hydraulic properties were determined by using the simplified evaporation method. Both unimodal and bimodal soil hydraulic functions were used in the analysis. The estimated parameters were then used in the HYDRUS-3D model to simulate a 2-mo-long period. Precipitation, irrigation, evaporation, and root water uptake processes were included in the numerical analysis. The values of 0.74 and 0.8 of the Nash–Sutcliffe efficiency index for the model predictions using unimodal and bimodal functions, respectively, confirmed the good agreement between the modeled and measured outflows. The bimodal model was able to both accurately reproduce the hydrographs in both dry and wet periods and account for daily fluctuations of soil moisture. Finally, the validated model was used to carry out a hydrological analysis of the green roof and its hydrological performance during the entire simulated period as well as during single precipitation events.

Core Ideas

- A comprehensive numerical analysis of hydrological processes in a green roof was conducted.
- The substrate of the green roof demonstrated bimodal behavior.
- The validated model accurately describes the hydraulic behavior of the green roof.
- The soil moisture governs the performance of the green roof during precipitation.

Abbreviations: AIC, Akaike information criterion; LID, low-impact development; NSE, Nash–Sutcliffe efficiency; RMSE, root mean square error; VGM, van Genuchten–Mualem.

During the last few decades, the area of impervious surfaces in urban areas has exponentially increased as a consequence of demographic growth. This long-term process has altered the natural hydrological cycle by reducing the infiltration and evaporation capacity of urban catchments, while increasing surface runoff and reducing groundwater recharge. Moreover, the frequency of extreme rainfall events, characterized by high intensity and short duration, is expected to increase in the near future as a consequence of global warming (Kundzewicz et al., 2006; Min et al., 2011).

The combined effects of urbanization and climate change expose urban areas to an increasing risk of flooding. In this context, urban drainage systems play a fundamental role in improving the resilience of cities. In recent years, an innovative approach to land development known as low-impact development (LID) has gained increasing popularity. Low-impact development is a "green" approach to storm water management that seeks to mimic the natural hydrology of a site using decentralized microscale control measures (Coffman, 2002). Low-impact development practices consist of bioretention cells, infiltration wells or trenches, stormwater wetlands, wet ponds, level spreaders, permeable pavements, swales, green roofs, vegetated filter and buffer strips, sand filters, smaller culverts, and water harvesting systems. Low-impact developments are able to reduce runoff

G. Brunetti and P. Piro, Dep. of Civil Engineering, Univ. of Calabria, Rende, CS 87036, Italy; J. Šimůnek, Dep. of Environmental Sciences, Univ. of California, Riverside, CA 92521. *Corresponding author (giuseppe.brunetti@unical.it).

Vadose Zone J.
doi:10.2136/vzj2016.04.0032
Received 19 April 2016.
Accepted 14 June 2016.

volumes and pollutant loads and increase evapotranspiration. Green roofs were able to significantly reduce peak rates of stormwater runoff (Getter et al., 2007) and retain rainfall volumes with retention efficiencies ranging from 40 to 80% (Bengtsson et al., 2004). Bioretention cells were shown to reduce average peak flows by at least 45% during a series of rainfall events in Maryland and North Carolina (Davis, 2008). Permeable pavements offered great advantages in terms of runoff reduction (Carbone et al., 2014; Collins et al., 2008), water retention, and water quality (Brattebo and Booth, 2003). Considering that rooftops may represent as much as 40 to 50% of the total impervious surfaces in urban areas, green roofs are among the key choices for hydrologic restoration and stormwater management.

One of the key factors limiting the widespread use of LIDs is the lack of adequate modeling tools (Elliott and Trowsdale, 2007) that could be used to design LIDs that function properly for particular climatic conditions. Low-impact development modeling requires an accurate description of the hydrological processes involved, which are multiple and interacting. In recent years, researchers have focused their attention on applying and developing empirical, conceptual, and physically based models for LID analysis. In their review, Li and Babcock (2014) reported that there were >600 studies published worldwide involving green roofs, with a significant portion of them related to modeling.

Zhang and Guo (2013) developed an analytical model to evaluate the long-term average hydrologic performance of green roofs. Local precipitation characteristics were described using probabilistic methods, and the hydrological behavior of the system was described using mass balance equations. Kasmin et al. (2010) developed a simple conceptual model of the hydrological behavior of green roofs during a storm event. The model input was the time series of precipitation events and the output was runoff. The water content in the green roof at any given time was between field capacity and the residual water content. Evapotranspiration was estimated using an empirical relationship accounting for the actual water contents, the storm event's characteristics, and the antecedent dry weather period. During a precipitation event, the porous medium absorbed moisture until field capacity was reached. The addition of further moisture produced subsurface flow.

She and Pang (2010) developed a physical model that combined an infiltration module (based on the Green–Ampt equation) and a saturation module (SWMM). The model calculates the water content in a green roof in a stepwise manner from the initiation of precipitation until saturation. In simulating the hydraulic response of green roofs to precipitation, an infiltration module is used before field capacity is reached and when no drainage is produced, while a saturation module is used after field capacity is reached and when drainage is produced. However, because runoff and infiltration can occur simultaneously during heavy precipitation, this stepwise approach may not be appropriate for a wide range of precipitation events.

Although analytical and conceptual models represent a viable alternative to the numerical analysis of green roofs, their use suffers from several limitations. Conceptualization of the physical processes involved often leads to simplification of the system and a reduction in numerical parameters. While in a physical model each parameter has its own meaning, in conceptual models, lumped parameters often incorporate different components of the described process. These lumped parameters are case sensitive and need to be calibrated against experimental data, implying a lack of generality of the model itself. These drawbacks could represent a barrier to the use of modeling tools among practitioners who need reliable and generally applicable models.

Mechanistic models have proven to be a valid and reliable alternative to conceptual and analytical models for the analysis of green roofs and LIDs in general. Carbone et al. (2015a) developed a one-dimensional finite volume model for description of the infiltration process during rainfall events in green roof substrates. The model was based on the reduced advective form of the Richards equation, in which the soil water diffusivity was neglected. Metselaar (2012) used the SWAP software (van Dam et al., 2008) to simulate the one-dimensional water balance of a substrate layer on a flat roof with plants. Hilten et al. (2008) simulated peak flow and runoff volume reduction of a 10-cm modular green roof (60 by 60 cm) using HYDRUS-1D (Šimůnek et al., 2008). In that study, only the values of field capacity and wilting point were measured. These parameters, in conjunction with the soil bulk density and particle size distribution, were used to estimate the soil water retention curve using a pedotransfer function. Multiple 24-h storms were used to generate precipitation data and simulate runoff to describe the green roof's hydrologic response. Li and Babcock (2015) used HYDRUS-2D to model the hydrologic response of a pilot 61- by 61-cm green roof system. Physical properties of the substrate were obtained using laboratory measurements on soil cores extracted from a green roof. The saturated hydraulic conductivity was measured using the falling-head method, while the residual and saturated water contents were measured using the gravimetric method. The hanging water column method was used to estimate the shape parameters of the unimodal van Genuchten function (van Genuchten, 1980). The model was calibrated using water content measurements obtained with time domain reflectometry sensors. The calibrated model was then used to simulate the potential beneficial effects of irrigation management on the reduction of runoff volumes.

Although physically based models have been widely and often successfully used, very few studies have provided a comprehensive analysis of the hydrological behavior of a green roof and validated it against field-scale data. Moreover, studies that investigated the unsaturated hydraulic properties of green roof substrates have been limited to the determination of some specific soil characteristics (e.g., field capacity, wilting point, or particle size distribution) and generally focused only on the soil water retention curves.

For these reasons, the aim of this study was an accurate and comprehensive analysis of the hydrological behavior of green roofs using the mechanistic model HYDRUS-3D to analyze an extensive green roof installed at the University of Calabria. The problem was addressed in the following way. First, the soil water retention curve and the unsaturated hydraulic conductivity of the green roof substrate were measured using a simplified evaporation method. The soil hydraulic parameters obtained were then used in HYDRUS-3D numerical simulations of the green roof function using precipitation, climate, and subsurface experimental data for a 2-mo-long period. The model was validated by comparing the modeled and measured subsurface flows using the Nash–Sutcliffe efficiency index (Nash and Sutcliffe, 1970). Finally, the validated model was used to evaluate the hydrologic behavior of the green roof and its hydraulic response to single precipitation events.

Materials and Methods

Green Roof and Site Description

The University of Calabria is located in the south of Italy, in the vicinity of Cosenza (39°18′ N, 16°15′ E). The climate is Mediterranean, with a mean annual temperature of 15.5°C and an average annual precipitation of 881.2 mm. The green roof is part of the "Urban Hydraulic Park," which also includes a permeable pavement, a bioretention system, and a sedimentation tank connected to a treatment unit. An extensive green roof was installed on the existing rooftop of the Department of Mechanical Engineering. The original impervious roof was divided into four sectors. Two sectors are vegetated with native plants and differ from each other by the drainage layer. Another sector is characterized by bare soil with only a few spontaneous plants. The last sector is the original impervious roof. The maximum depth of the soil substrate is 8 cm. This depth was selected to investigate both the energetic (heat fluxes) and hydrologic (water fluxes) behavior of a very thin extensive green roof under the Mediterranean climate. The soil substrate is composed of mineral soil with 74% gravel, 22% sand, and 4% silt and clay. The soil has a measured bulk density of 0.86 g cm^{-3} and 8% organic matter, which was determined in the laboratory using the Walkley–Black method. Three different plant species were selected and planted. *Cerastium tomentosum* L. and *Dianthus gratianopolitanus* Vill. are herbaceous plants suited for well-drained soils; *Carpobrotus edulis* (L.) L. Bolus is a succulent plant characterized by a high drought tolerance, largely due to the high leaf succulence and physiological adaptations such as crassulacean acid metabolism (CAM) photosynthesis (Durhman et al., 2006); CAM plants have greater water use efficiency than C_3 plants because their transpiration per unit of CO_2 is reduced due to the stomata opening at night for CO_2 uptake (Sayed, 2001).

In this study, only one vegetated sector of the green roof was considered. Figure 1 displays a cross-section of the green roof; the considered sector has an area of 50 m^2 and an average slope of 1%. The green roof is divided into square elements of 50 by 50 cm (Fig. 2), with alternating vegetated and non-vegetated areas. The substrate has a maximum depth of 8 cm where plants are grown and a minimum depth of 4 cm where no vegetation is present (Fig. 1 and 2). This design was meant to minimize the weight on the green roof support structure. A highly permeable geotextile is placed at the bottom of the substrate to prevent soil from migrating into the underlying layers. The drainage layer is composed of a polystyrene foam and is characterized by a water storage capacity of 11 L m^{-2} and a drainage capacity of 0.46 L s^{-1} m^{-2}. Water accumulated in the drainage layer can be transferred back up to the substrate only by condensation on the geotextile. An anti-root layer and an impervious membrane complete the green roof.

A drip irrigation system was installed to provide water to the plants during drought periods. The irrigation system is connected with a reuse system, which collects outflow from the green roof. Only reused water was used for irrigating the green roof. The reuse system is composed of a storage tank and a pump. When the storage capacity of the tank (1.5 m^3) is exceeded, water is directly discharged into the drainage system. Drippers are located at the center of each square, and their distance from each other is approximately 50 cm. Drippers were also installed in non-vegetated areas to utilize water from the storage tank by using the evapotranspiration capacity of the green roof. In this way, the volume of water discharged into the drainage system is reduced, and the evaporative cooling effect of the green roof on the building is expected

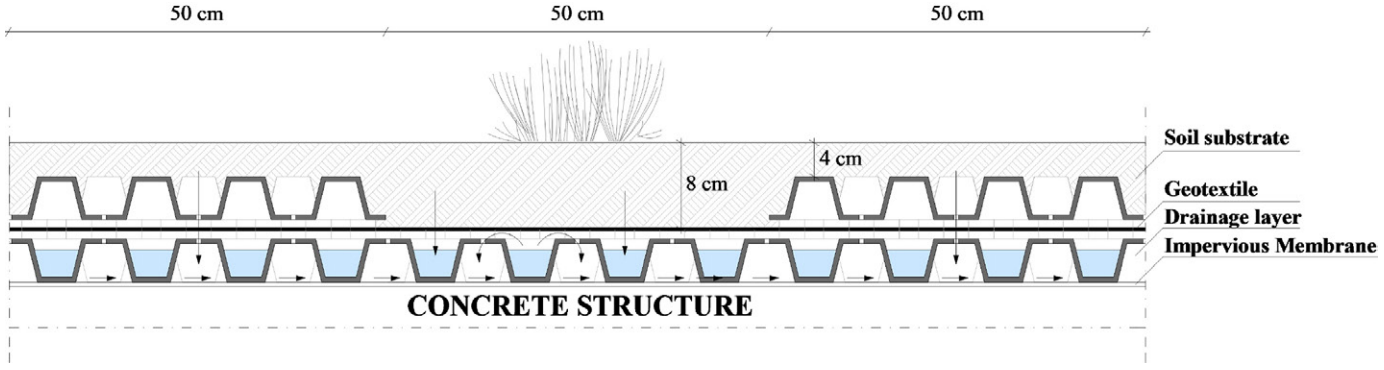

Fig. 1. A typical cross-section of the green roof.

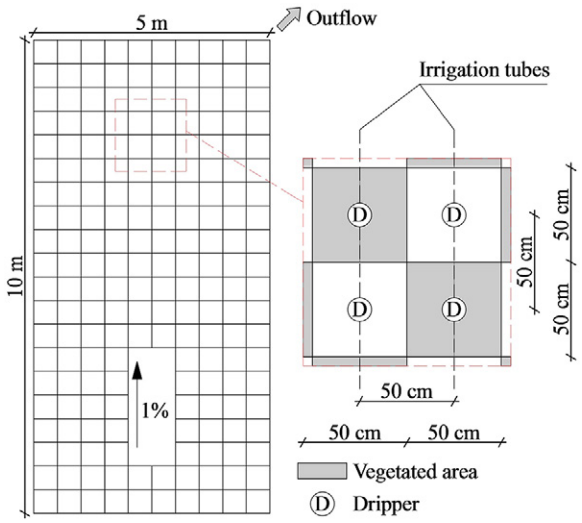

Fig. 2. A schematic of the green roof, showing both vegetated (gray) and non-vegetated (white) areas.

to increase. The irrigation system is activated at predefined times by an electric valve, and the irrigation rate is measured by a water counter with an acquisition frequency of 1 min. The total volume of irrigation for the selected time period was 142 mm.

A weather station located directly at the site measured precipitation, velocity and direction of wind, air humidity, air temperature, atmospheric pressure, and global solar radiation. Precipitation was measured using a tipping bucket rain gauge with a resolution of 0.254 mm and an acquisition frequency of 1 min. Climatic data were acquired with a frequency of 5 min. Data were processed and stored in a SQL database.

A flux meter located at the base of the building, composed of a polyvinyl chloride (PVC) pipe with a sharp-crested weir and a pressure transducer, measured outflow from the green roof. The pressure transducer (Ge Druck PTX1830) measured the water level inside the PVC pipe and had a measurement range of 75 cm, with an accuracy of 0.1% of the full scale. The pressure transducer was calibrated in the laboratory using a hydrostatic water column, linking the electric current intensity with the water level inside the column. The exponential head-discharge equation for the flux meters was obtained by fitting the experimental data. The subsurface flow data were acquired with a time resolution of 1 min and stored in a SQLITE database.

A 2-mo data set was selected for analysis (Fig. 3). This particular time period, which started on 1 Sept. 2015 and ended on 30 Oct. 2015, was selected because it involved highly variable climatic conditions. Isolated precipitation occurred in September, which had a relatively high average temperature. These climatic conditions required irrigation of the green roof for 1 h during the night. October was characterized by intense and frequent precipitation events. The total recorded precipitation for the whole period was 431 mm, with an average air temperature of 20.2°C.

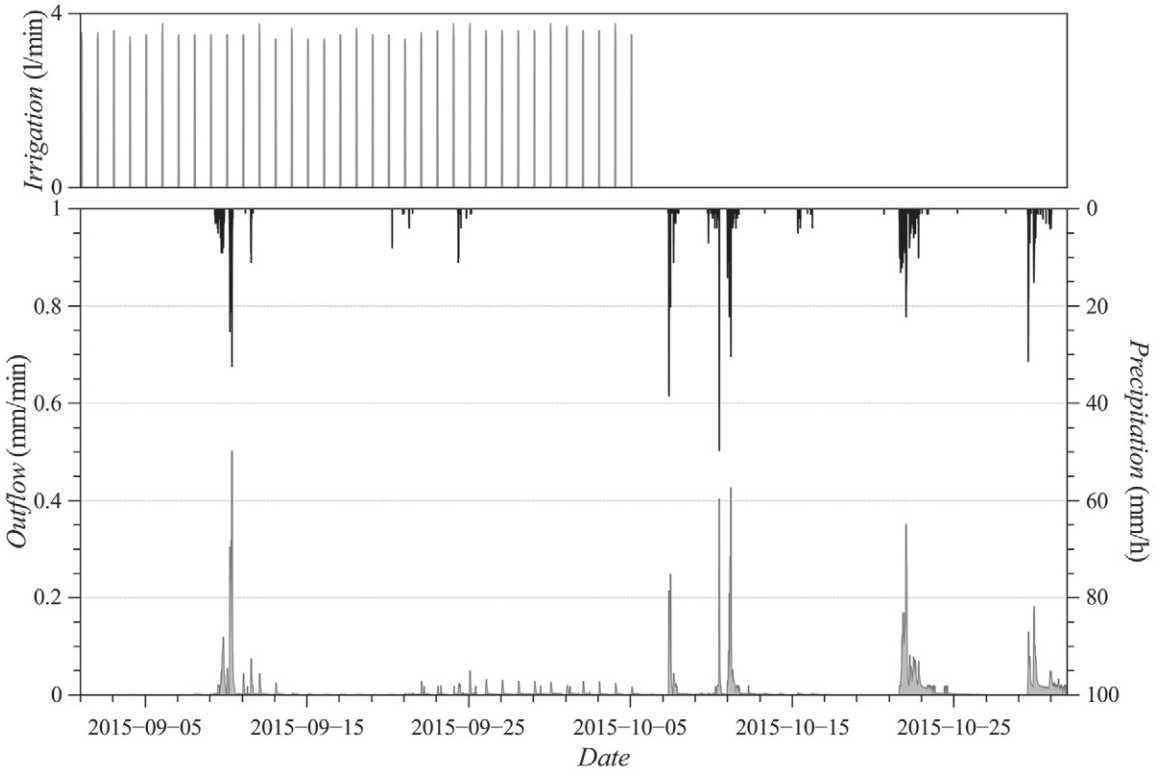

Fig. 3. Measured precipitation (black), irrigation (top), and subsurface (gray) fluxes for a selected time period in September and October 2015.

Hourly reference evapotranspiration was calculated using the Penman–Monteith equation (Allen et al., 1998). An average albedo value of 0.2 was used in calculations of net shortwave radiation, assuming that the albedo for vegetated areas was 0.23 (Lazzarin et al., 2005) and 0.17 for bare soil (Rosenberg et al., 1983).

Soil Hydraulic Properties

Evaporation Method

Modeling of water flow in unsaturated soils by means of the Richards equation requires knowledge of the water retention function, $\theta(h)$, and the hydraulic conductivity function, $K(h)$, for each soil layer of the green roof, where θ is the volumetric water content [$L^3\ L^{-3}$], h is the pressure head [L], and K is the hydraulic conductivity [$L\ T^{-1}$]. A broad range of methods exists for the determination of soil hydraulic properties in the field or in the laboratory (Arya, 2002; Dane and Hopmans, 2002; Klute and Dirksen, 1986). The numerical inversion of transient flow experiments represents one of the most accurate ways to determine soil hydraulic properties (Šimůnek et al., 1998). Among these, the simplified evaporation method (Schindler, 1980) is one of the most popular methods. Peters and Durner (2008) conducted a comprehensive error analysis of the simplified evaporation method and concluded that it is a fast, accurate, and reliable method to determine soil hydraulic properties in the measured pressure head range and that the linearization hypothesis introduced by Schindler (1980) causes only small errors. The evaporation method was further modified by Schindler et al. (2010a, 2010b) to significantly extend the measurement range to higher pressures. For a detailed description of the modified evaporation method, please see Schindler et al. (2010a, 2010b).

A drawback of the evaporation method is that it remains unsuited for direct determinations of conductivities near saturation (Wendroth et al., 1993). The determination of hydraulic conductivities remains reliable only in the dry range, in which hydraulic gradients are more pronounced. To improve the characterization of the hydraulic conductivity function near saturation, alternative methods are required such as the multistep outflow method (Peters and Durner, 2008).

In this study, the simplified evaporation method with the extended measurement range (down to −9000 cm) was used for the determination of the unsaturated hydraulic properties of the green roof substrate. For a complete description of the system, please see UMS GmbH (2015). The soil for the laboratory analysis was sampled directly from the green roof using a stainless-steel sampling ring with a volume of 250 mL. The soil sample was saturated from the bottom before starting the evaporation test. The measurement unit and tensiometers were degassed using a vacuum pump to reduce the potential nucleation sites in the demineralized water. Because Peters and Durner (2008) suggested a reading interval for structured soils of <0.1 d, the reading interval was set to 20 min to have high-resolution measurements. At the end of the experiment, the sample was placed in an oven at 105°C for 24 h, and then the dry weight was measured.

Parameter Estimation

The numerical optimization procedure HYPROP-FIT (Pertassek et al., 2015) was used to simultaneously fit retention and hydraulic conductivity functions to the experimental data obtained using the evaporation method. HYPROP-FIT is a computer program designed to fit unimodal and multimodal retention functions to measured water retention data and to compute the corresponding relative hydraulic conductivity function. The fitting is accomplished by a nonlinear optimization algorithm that minimizes the sum of weighted squared residuals between model predictions and measurements. The software uses the Shuffled Complex Evolution algorithm proposed by Duan et al. (1992), which is a global parameter estimation algorithm. The software includes a corrected fit of the hydraulic functions by the "integral method" to avoid bias in the hydraulic properties near saturation (Peters and Durner, 2006), an Hermitian spline interpolation of the raw measured data to obtain smooth and continuous time series of measured data, and automatic detection of the validity range of conductivity data near saturation, where the hydraulic gradients become too small to yield reliable data.

Two different models were evaluated for the description of soil hydraulic properties. The unimodal van Genuchten–Mualem (VGM) model (van Genuchten, 1980) was used first:

$$\Theta = \begin{cases} \dfrac{1}{\left[1+\left(\alpha|h|\right)^n\right]^m} & \text{if } h \le 0 \\ 1 & \text{if } h > 0 \end{cases} \qquad [1]$$

$$\Theta = \frac{\theta - \theta_r}{\theta_s - \theta_r}$$

$$K = \begin{cases} K_s \Theta^L \left\{\left[1-\left(1-\Theta^{1/m}\right)\right]^m\right\}^2 & \text{if } h < 0 \\ K_s & \text{if } h > 0 \end{cases} \qquad [2]$$

$$m = 1 - \frac{1}{n}$$

where Θ is the effective saturation (dimensionless), α is a parameter related to the inverse of the air-entry pressure head [L^{-1}], θ_s and θ_r are the saturated and residual water contents, respectively (dimensionless), n and m are pore-size distribution indices (dimensionless), K_s is the saturated hydraulic conductivity [$L\ T^{-1}$], and L is the tortuosity and pore-connectivity parameter (dimensionless).

Because the unimodal VGM model cannot always describe the full complexity of measured data, the bimodal model of Durner (1994), which constructs the retention and hydraulic conductivity functions by a linear superposition of two or more VGM functions, was used next:

$$\Theta=\begin{cases}\sum_{i=1}^{2} w_i \left\{\dfrac{1}{\left[1+\left(\alpha_i|h|\right)^{n_i}\right]^{m_i}}\right\} & \text{if } h<0\\ 1 & \text{if } h>0\end{cases} \quad [3]$$

$$K=\begin{cases}K_s\left(\sum_{i=1}^{2} w_i\Theta_i\right)^{L}\left\{\dfrac{\sum_{i=1}^{2} w_i\alpha_i\left[1-\left(\alpha_i|h|\right)^{n_i}\Theta_i\right]}{\sum_{i=1}^{2} w_i\alpha_i}\right\}^{2} & \text{if } h<0\\ K_s & \text{if } h>0\end{cases} \quad [4]$$

where w is a weighting factor and i refers to the ith pore system.

Although the K_s value is commonly fixed to the measured value of the saturated hydraulic conductivity, some studies have showed that this can introduce bias in the unsaturated hydraulic conductivity function when using the traditional VGM model. Schaap and Leij (2000) and Schaap et al. (2001) confirmed that fixing K_s to a measured value of the saturated hydraulic conductivity led to a systematic overestimation of the hydraulic conductivity at most pressure heads. Furthermore, Schaap et al. (2001) demonstrated that the hydraulic conductivity estimated by fitting K_s provided a much better description of the hydraulic conductivity at negative pressure heads than fixing it at the measured saturated hydraulic conductivity. In addition, Schaap and Leij (2000) found that the fitted value of the tortuosity L was often negative, with an optimal value of −1. For these reasons, all the parameters were initially included in the optimization.

The goodness-of-fit was evaluated in terms of the root mean square error (RMSE), while the Akaike information criterion (AIC) (Hu, 1987) was used to choose between different hydraulic conductivity functions with different numbers of optimized parameters. The software also provides 95% confidence intervals to assess the uncertainty in parameter estimation.

Modeling Theory

Water Flow and Root Water Uptake

The HYDRUS-3D software (Šimůnek et al., 2008) was used to describe the morphological complexity of the green roof, which simultaneously includes multiple soil depths, both vegetated and non-vegetated areas, and drip irrigation. The green roof consists of four square elements, which are regularly repeated (Fig. 2). The hydrologic response of the entire green roof can be well described as a superposition of the behavior of these four elements.

HYDRUS-3D is a three-dimensional model for simulating the movement of water, heat, and multiple solutes in variably saturated porous media. HYDRUS-3D numerically solves the Richards equation for multidimensional unsaturated flow:

$$\frac{\partial\theta}{\partial t}=\nabla\left[K\nabla(h-z)\right]-S \quad [5]$$

where S is a sink term [$L^3\ L^{-3}\ T^{-1}$], defined as a volume of water removed from a unit volume of soil per unit of time due to plant water uptake. Feddes et al. (1978) defined S as

$$S(h)=a(h)S_p \quad [6]$$

where $a(h)$ is a dimensionless water stress response function that depends on the soil pressure head h and has a range of values between 0 and 1, and S_p is the potential root water uptake rate. Feddes et al. (1978) proposed a water stress response function, in which water uptake is assumed to be zero close to soil saturation (h_1) and for pressure heads higher (in absolute values) than the wilting point (h_5). Water uptake is assumed to be optimal between two specific pressure heads (h_2, h_3, or h_4), which depend on a particular plant. At high potential transpiration rates (5 mm d^{-1} in the model simulation), stomata start to close at lower pressure heads (h_3) (in absolute value) than at low potential transpiration rates (1 mm d^{-1}) (h_4). Parameters of the stress response function for a majority of agricultural crops can be found in various databases (e.g., Taylor and Ashcroft, 1972; Wesseling et al., 1991).

As explained above, green roof plants were selected to suit Mediterranean climate conditions. Hanscom and Ting (1978) conducted a comprehensive experimental campaign on the behavior of succulent plants under water stress. They observed that during time periods with water and salt stress, plants closed their stomata and, as a consequence, little or no transpiration occurred even during daylight hours. Thus, the plants were capable of withstanding extended periods of drought. In the same study, well-watered plants exhibited normal C_3 photosynthesis mechanisms, with the maximum CO_2 uptake occurring during the day. This behavior was reported also by Starry et al. (2014). Considering that the combined effects of irrigation and precipitation limited the drought periods, it appears reasonable to assume that a normal C_3 mechanism occurred. For these reasons, the parameters reported by Wesseling et al. (1991) for pasture were slightly modified in this study. In particular, h_1 and h_2 were set to −1 and −10 cm, respectively, to increase actual transpiration for near-saturated conditions. Parameters used in the water stress response function are reported in Table 1.

The local potential root water uptake S_p was calculated from the potential transpiration rate T_p. Beer's equation was first used

Table 1. Feddes' parameters for the water stress response function used in numerical simulations.

Feddes' parameter	Pressure head
	cm
h_1	−1
h_2	−10
h_3	−200
h_4	−800
h_5	−8000

to partition reference evapotranspiration, calculated using the Penman–Monteith equation (Allen et al., 1998), into potential transpiration and potential soil evaporation fluxes (e. g., Ritchie, 1972). The leaf area index (LAI) is needed to partition evaporation and transpiration fluxes. In this study, a LAI value of 2.29 as reported by Blanusa et al. (2013) for a *Sedum* mix was used in vegetated areas. For a detailed explanation of evapotranspiration partitioning, please see Sutanto et al. (2012).

As described above, the vegetated and non-vegetated green roof elements alternate, while plants are located in the center of vegetated areas. HYDRUS-3D allows the consideration of a spatially variable root distribution. A cylinder with a radius of 20 cm and a depth of 8 cm, in the center of the vegetated area, was used to model the root zone. The root density was assumed to be uniform inside the cylinder and zero in the remaining part of the numerical domain. The total potential transpiration flux from a transport domain is, in HYDRUS, equal to potential transpiration T_p multiplied by the surface area associated with vegetation. This total potential transpiration flux is then distributed throughout the entire root zone for the computation of the actual root water uptake.

Numerical Domain and Boundary Conditions

The two main elements that form a green roof are the soil substrate and the drainage layer. While the role of the substrate is well known because it governs the dynamics of infiltration and evapotranspiration, the importance of the drainage layer for the hydraulic behavior of a green roof is only partially described in the literature, especially with respect to the modeling of its function. The drainage layer is frequently modeled as an open reservoir (e.g., Locatelli et al., 2014; Vesuviano et al., 2014). Once the drainage layer's storage capacity is reached, the excess water is drained through holes into outflow drains. This guarantees a high permeability of the system and avoids the formation of ponding on top of the substrate layer even for intense precipitation. An open space of 1 cm separates the soil substrate and drainage holes (Fig. 1 and 4).

Water accumulated in the drainage layer can return to the soil substrate only by evaporation and subsequent condensation on the geotextile at the bottom of the soil. In this small air space, potential evaporation is expected to be limited due to the microclimatic conditions to which water in the drainage layer is exposed. The enclosed air space is expected to be characterized by relatively high humidity, considering the combined effects of soil moisture and the vicinity of the water table of the drainage layer. Moreover, radiation and air turbulence can be considered negligible in this enclosed air space. The only factors that can thus produce evaporation are the air temperature and air humidity. However, the above considerations suggest that the effects of evaporation and microcondensation can be neglected, especially at the field scale. This implies that variations in the water level in the drainage layer are limited and, consequently, the storage capacity of the drainage

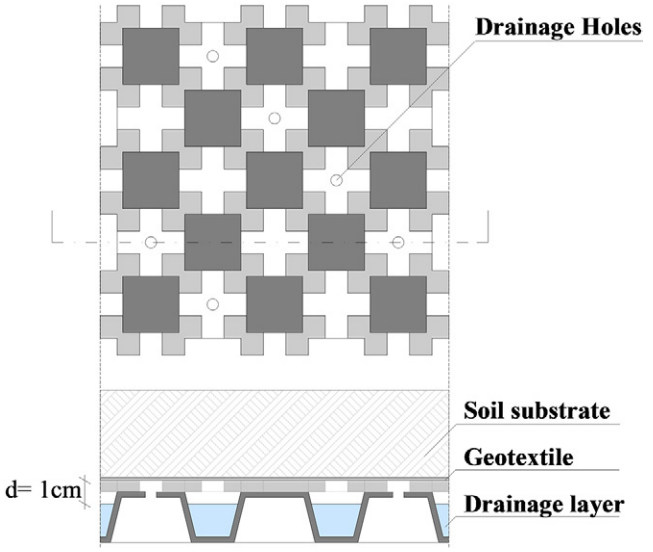

Fig. 4. Details of the drainage layer, where d is the thickness of the open space between drainage holes, and the geotextile supporting the green roof substrate.

layer has only a limited effect on green roof outflow. For these reasons, only the soil substrate was modeled in this study.

While precipitation and potential evaporation (different in vegetated and bare areas; see Table 2) were uniformly distributed on the soil surface, the drip irrigation was modeled at predefined surface points. Drippers can be idealized as point sources with a specified irrigation flux. However, if the irrigation flux is applied to a single boundary node and this flux exceeds the infiltration capacity of this node, problems with numerical convergence can occur. To avoid such numerical problems, the irrigation flux should be distributed across a larger surface area, which should ideally represent the wetting radius. This area must be large enough to avoid surface ponding. In this study, the irrigation flux was distributed across a circular area with a radius of 5 cm located in the center of each element. As a result, no ponding was observed during numerical simulations.

The surface of the green roof was thus exposed to precipitation, evaporation, and irrigation. As a result, three different boundary

Table 2. Fluxes considered under different types of boundary conditions.

Boundary condition	Flux†
Atmospheric	precipitation, potential evaporation (= $ET_0 f$), and potential transpiration [= $ET_0(1-f)$]
Variable flux 1	precipitation and potential evaporation
Variable flux 2	precipitation, irrigation, potential evaporation (= $ET_0 f$), and potential transpiration [= $ET_0(1-f)$]
Seepage face	seepage
Zero flux	no flux

† ET_0, reference evapotranspiration; f, distribution coefficient dependent on the leaf area index (Ritchie, 1972).

conditions were specified at the surface of the modeled domain and two boundary conditions at its bottom (Fig. 5). Table 2 summarizes the various fluxes considered in the various types of used boundary conditions.

The "atmospheric" boundary condition, which was assigned to areas under vegetation, can exist in three different states: (i) precipitation and/or potential evaporation fluxes, (ii) a zero pressure head (full saturation) during ponding when both infiltration and surface runoff occurs, and (iii) an equilibrium between the soil surface pressure head and the atmospheric water vapor pressure head when atmospheric evaporative demand cannot be met by the substrate. The threshold pressure head, which was set to −30,000 cm, divides the evaporation process from the soil surface into two stages: (i) a constant-rate stage when actual evaporation, equal to potential evaporation, is limited only by the supply of energy to the surface, and (ii) the falling-rate stage when water movement to the evaporating sites near the surface is controlled by subsurface soil moisture and the soil hydraulic properties and when actual evaporation, calculated as a result of the numerical solution of the Richards equation, is smaller than potential evaporation.

A special option of HYDRUS-3D was used to treat the "variable flux" boundary conditions as the "atmospheric" boundary conditions (i.e., with the limiting pressure heads described above). The Variable Flux 1 boundary condition included precipitation and potential evaporation and was assigned to bare soil areas. Because no vegetation was present in these areas, the reference evapotranspiration was not partitioned as for the "atmospheric" boundary condition but was fully assigned to potential evaporation. This approach shares some similarities with the "dual" crop coefficient introduced by Allen et al. (1998):

$$ET_c = ET_0\left(K_{cb} + K_e\right) \quad [7]$$

where ET_c is the actual crop evapotranspiration, ET_0 is the reference evapotranspiration, K_{cb} is the basal crop coefficient, and K_e is the empirical soil evaporation coefficient, which accounts for multiple factors affecting soil evaporation, such as soil texture and available soil moisture. In the case of bare soil, K_{cb} becomes zero because no vegetation is present and ET_c is related only to the soil evaporation coefficient (Torres and Calera, 2010). In HYDRUS, soil evaporation is modeled using the two-stage model with the threshold pressure head (described above), which directly accounts for factors affecting soil evaporation and which thus does not require the use of K_e.

The Variable Flux 2 boundary condition, which involved precipitation, irrigation, and evaporation, was applied to the circular areas with a radius of 5 cm where drippers were located.

A seepage-face boundary condition was specified at the bottom of the soil substrate under vegetated areas because the geotextile is exposed to atmospheric pressure. A seepage-face boundary acts as a zero pressure head boundary when the boundary node is saturated and as a no-flux boundary when it is unsaturated. In non-vegetated elements, a zero flux boundary condition was applied, except in small circular areas that represented drainage holes (Fig. 1 and 4). Three circular areas, each with a radius of 0.5 cm at the bottom of the non-vegetated elements, were modeled as seepage faces. Considering the occurrence of high nonlinearities and fluxes around these drainage holes, the finite element mesh was refined here (to 0.5 cm) to guarantee a good accuracy of the numerical solution. No-flux boundary conditions were used at the remaining boundaries.

The initial pressure head was assumed to be constant in the entire domain and was set equal to −330 cm, which is usually assumed to be the field capacity. The numerical model is expected to be sensitive to the initial condition only during the first few simulated days.

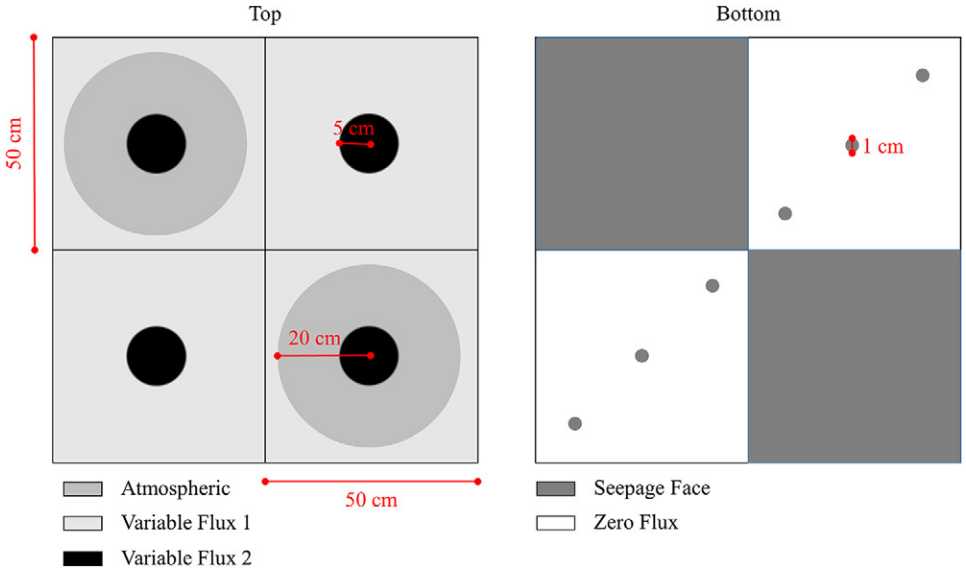

Fig. 5. Spatial distribution of considered boundary conditions.

The three-dimensional simulated domain had a surface area of 1 m^2, a maximum height of 8 cm, and a total volume of 0.06 m^3. The domain was discretized into three-dimensional prismatic elements using the MESHGEN Plus tool of HYDRUS-3D. No mesh stretching was used, and the finite element (FE) mesh was isotropic. The generated FE mesh had 10,709 nodes and 49,027 three-dimensional elements. The quality of the FE mesh was assessed by checking the mass balance error reported by HYDRUS-3D at the end of the simulation. Mass balance errors, which in this simulation were always <1%, are generally considered acceptable at these low levels.

Statistical Evaluation

The Nash–Sutcliffe efficiency (NSE) index (Nash and Sutcliffe, 1970) was used to evaluate the agreement between measured and modeled hydrographs:

$$\mathrm{NSE} = 1 - \left[\frac{\sum_{i=1}^{T} \left(Q_i^{\mathrm{obs}} - Q_i^{\mathrm{mod}} \right)^2}{\sum_{i=1}^{T} \left(Q_i^{\mathrm{obs}} - Q_{\mathrm{mean}}^{\mathrm{obs}} \right)^2} \right] \quad [8]$$

where T is the total number of observations, Q_i^{obs} is the ith measured value, Q_i^{mod} is the ith simulated value, and $Q_{\mathrm{mean}}^{\mathrm{obs}}$ is the mean value of the observed data. The NSE index ranges between $-\infty$ and 1.0, is equal to 1 in the case of a perfect agreement, and generally, values between 0.0 and 1.0 are considered acceptable (Moriasi et al., 2007). The NSE index was used because it is often reported to be a valid indicator for evaluating the overall fit of a hydrograph (Servat and Dezetter, 1991).

Results and Discussion

Soil Hydraulic Properties

Soil hydraulic properties measured using the evaporation method are displayed in Fig. 6. The soil water retention curve is well described across the entire water content range (Fig. 6). The retention data point close to $\log(h) = 4$ (h in cm) was obtained by using the air-entry pressure head of the ceramic. At first inspection, the behavior of the retention curve appears not to be perfectly sigmoidal, which may indicate the presence of a secondary pore system (Durner, 1994). Measured points of the hydraulic conductivity function are concentrated in the dry range between 10 and 30% of the volumetric water content. This is common when the evaporation method is used to measure soil hydraulic properties of coarse-textured soils such as the substrate of the green roof.

The measured data were imported into the HYPROP-FIT software to fit the analytical hydraulic property functions. The unimodal VGM model (van Genuchten, 1980) was fitted first. The RMSE values for retention and conductivity functions were 0.02 $cm^3\ cm^{-3}$ and 0.13 (in log K, cm d^{-1}), respectively. An AIC of −874 was obtained when L was included in the optimization. The unimodal function introduced a high bias, especially in the hydraulic conductivity function. The bimodal Durner (1994) model (Eq. [3–4]) was fitted next. The RMSE values for the retention and conductivity functions were 0.005 $cm^3\ cm^{-3}$) and 0.07 (in log K, cm d^{-1}), respectively. An AIC of −1298 was obtained when the value of L was fixed to 0.5, as this is the value usually assumed in the literature for many soils. Figure 6 displays a comparison between the measured data and their fit using the unimodal and bimodal retention functions. The estimated soil hydraulic parameters with their confidence intervals are reported in Table 3.

It is evident that the bimodal function provides a more accurate description of the retention curve. A significant difference between unimodal and bimodal functions emerges in the dry range between $\log(h) = 4$ and 6, where the unimodal function estimates lower water contents. The unimodal function overestimates

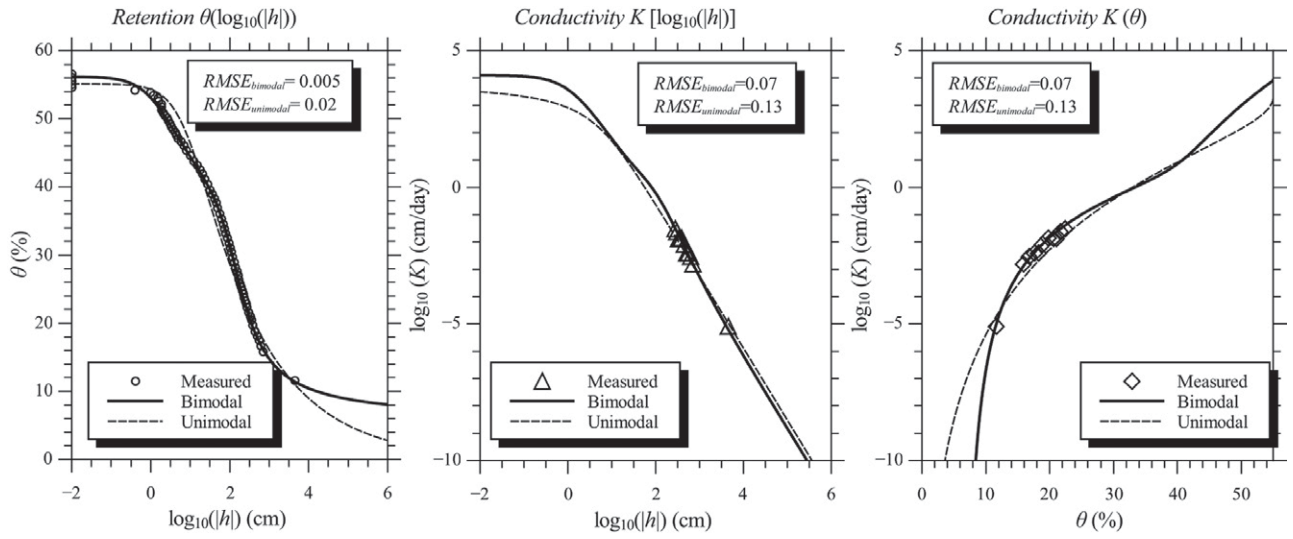

Fig. 6. Measured and modeled values of the retention curve θ[$\log_{10}(h)$] (left) and the hydraulic conductivity functions K[$\log_{10}(h)$] (center) and K(θ) (right). The measured values are scatter points; the solid and dashed lines are the fitted bimodal and unimodal functions, respectively.

Table 3. Estimated soil hydraulic parameters and their confidence intervals (CIs) for the unimodal and bimodal hydraulic functions.

	Unimodal		Bimodal	
Parameter	Estimation	CI	Estimation	CI
Residual water content (θ_r)	0	0.05	0.070	0.007
Saturated water content (θ_s)	0.551	0.01	0.562	0.003
Air-entry pressure head index for the first pore system (α_1), cm^{-1}	0.13	0.03	0.843	0.07
Pore-size distribution index for the first pore system (n_1)	1.25	0.06	1.24	0.04
Saturated hydraulic conductivity (K_s), cm d^{-1}	4700	3500	12600	3700
Air-entry pressure index for the secondary pore system (α_2), cm^{-1}	–	–	0.01	0.001
Pore-size distribution index for the secondary pore system (n_2)	–	–	1.97	0.08
Weight coefficient (w_2)	–	–	0.422	0.01
Tortuosity and pore connectivity parameter (L)	0.53	0.02	0.5	–

the water contents in the range between $\log(h) = 0$ and 2 (h in cm). This is confirmed by the RMSE values, which are higher for the unimodal function, especially for the hydraulic conductivity function, for which the RMSE value is twice as large as for the bimodal function. The AIC value is higher (in absolute values) for the bimodal function, indicating that the model is better suited to describe the soil hydraulic properties of the evaluated soil than the unimodal model. Figure 6 displays measured data and the fitted multimodal retention and conductivity curves.

The change in the slope of the retention curve near saturation is reflected in the hydraulic conductivity function. However, this decrease in the hydraulic conductivity is not highly pronounced. Significant differences between the two hydraulic conductivity models occur only near saturation and in the dry range. The unimodal model estimates significantly lower hydraulic conductivity values close to saturation than the bimodal model. While the fitted saturated water contents θ_s are almost the same for both models, significant differences exist in the residual water contents θ_r. Fitted values of θ_r are 0.0 and 0.062 for the unimodal and bimodal models, respectively. The value estimated by the unimodal model seems unrealistically low, and it could indicate inaccuracy in the description of the soil hydraulic properties in the dry range.

Both models indicate a soil characterized by very high permeability, which corresponds well with the textural composition of the green roof substrate. This characteristic is well suited for green roof substrates, which must guarantee fast drainage and avoid water ponding on the surface even during intense precipitation. The volumetric water contents corresponding to field capacity and the wilting point were 21 and 10%, respectively, for the bimodal model and 21 and 8%, respectively, for the unimodal model.

The maximum correlation between optimized parameters for the bimodal model was 0.88 for θ_r and n_1, a result that is quite common when only a few points are measured in the dry range. However, only five correlation coefficients were >0.8, indicating a generally well-posed problem. On the other hand, the maximum correlation coefficient for the unimodal model was 0.97 for θ_r and n, which indicates ill-posedness of the optimization problem. Narrow confidence intervals for the parameters θ_r, θ_s, n_1, α_2, n_2, and w_2 indicate high confidence in their estimation. The fitted saturated hydraulic conductivity K_s and the parameter α_1 for the first pore system exhibited the largest uncertainties. As explained above, the evaporation method is not accurate for the determination of the hydraulic conductivity near saturation, and this fact is reflected in the estimation of K_s. To improve the accuracy in the estimation of the hydraulic conductivity near saturation, other methods should be used.

The above discussed analysis suggests that the bimodal model could provide a slightly better description of the soil hydraulic properties than the unimodal model.

Model Validation

Parameters obtained with the evaporation method were used in HYDRUS-3D to describe the soil hydraulic properties of the green roof substrate. Figure 7 shows a comparison between measured and simulated outflows from the green roof when using both unimodal and bimodal functions of soil hydraulic properties.

The NSE indices for measured and simulated green roof outflows were 0.74 and 0.8 when the unimodal and bimodal functions were used, respectively. These values indicate that both models were able to accurately describe the hydraulic behavior of the green roof, while a higher accuracy was achieved by the bimodal model. It is evident from Fig. 7 that the unimodal model failed in reproducing small outflows after irrigation, which were observed at the beginning and at the end of September. The inserts in Fig. 7 show simulated vs. measured green roof outflows. The same plot also shows a bisector line, which indicates a perfect agreement between simulated and measured outflows, and a linear regression line. The good performance of the models are confirmed by the coefficient of determination $R^2 = 0.85$ and 0.82 of the linear regressions for

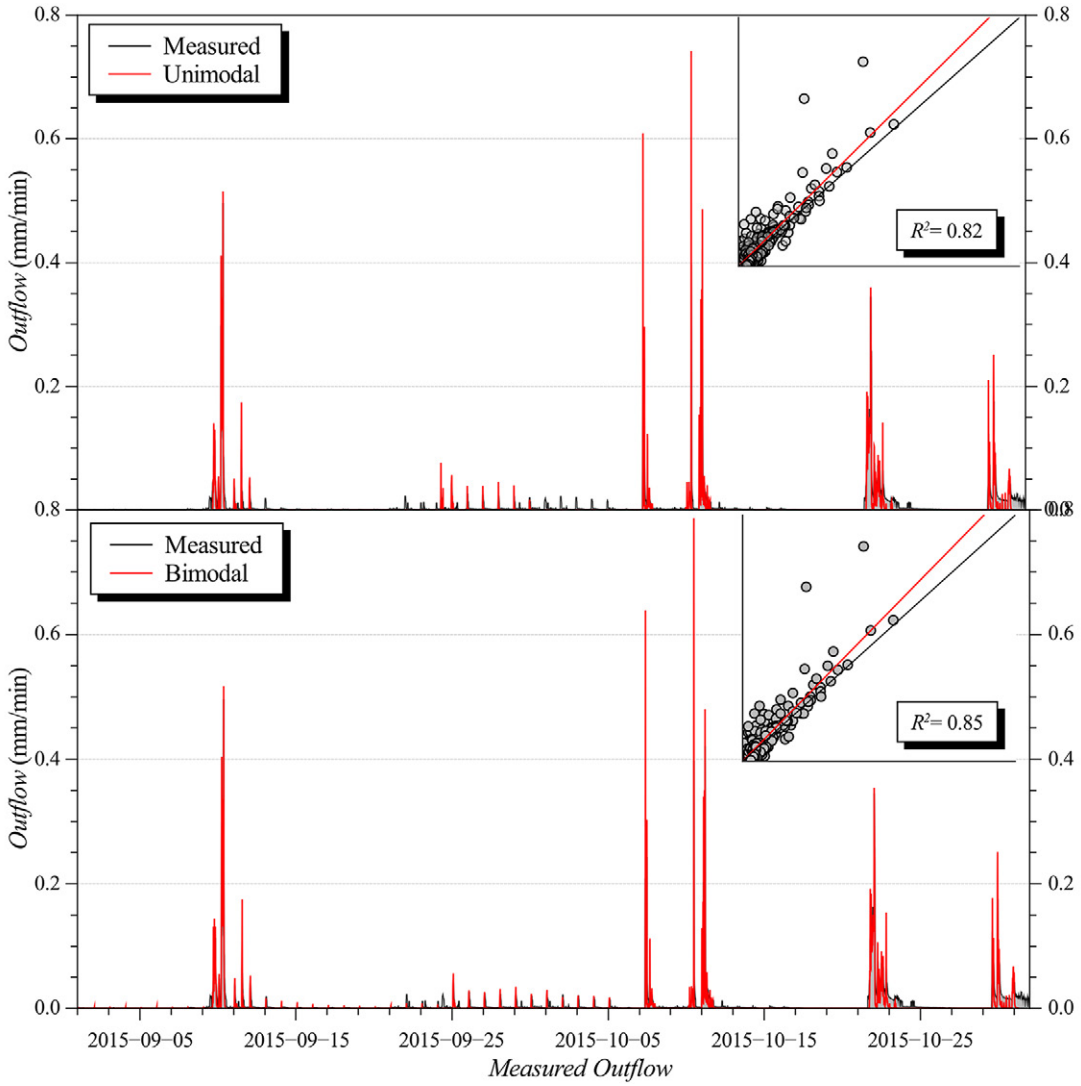

Fig. 7. A comparison between measured and simulated outflows vs. time for selected dates in September and October 2015 and against each other (in the insert). The red and black lines in the insert are bisector and linear regression lines, respectively.

the bimodal and unimodal models, respectively. The comparison between bisector and regression lines indicates that both models slightly overestimated the outflow.

A further analysis of the fit between measured and simulated green roof outflows was performed by analysis of the residuals, which is displayed in Fig. 8 using a lag plot. The lag plot is constructed by comparing neighboring residuals with respect to time (i and i – 1), where i is time with a measured value. A lag plot is useful for examining the dependency of the error terms. Any non-random pattern in a lag plot suggests that the variance is not random. No particular pattern emerges from analysis of the lag plot, suggesting that the errors are random for both the unimodal and bimodal functions (Fig. 8).

The bimodal model performed well during both dry and wet periods. In September, which was characterized by sparse precipitation, significant evapotranspiration, and daily irrigation, the model was able to reproduce both the fast response of the green roof to precipitation and the small response to drip irrigation. This also indicates good accuracy in the estimation of daily fluctuations in soil water contents due to the combined effects of both evaporation and root water uptake.

The overestimation of the peak flux values (Fig. 7) can be related to the combined effects of uncertainties in measured precipitation and estimated unsaturated hydraulic conductivity. During large precipitation events, a significant part of the domain near the geotextile (a seepage face) becomes saturated or nearly saturated, and under such conditions the hydraulic conductivity plays a fundamental role in the infiltration process. Considering the uncertainty and a possible bias introduced by the evaporation method for hydraulic conductivity values near saturation, it is reasonable to assume that the errors in the predicted peak fluxes are related to this uncertainty. A more accurate description of the hydraulic conductivity close to saturation should help in improving the accuracy

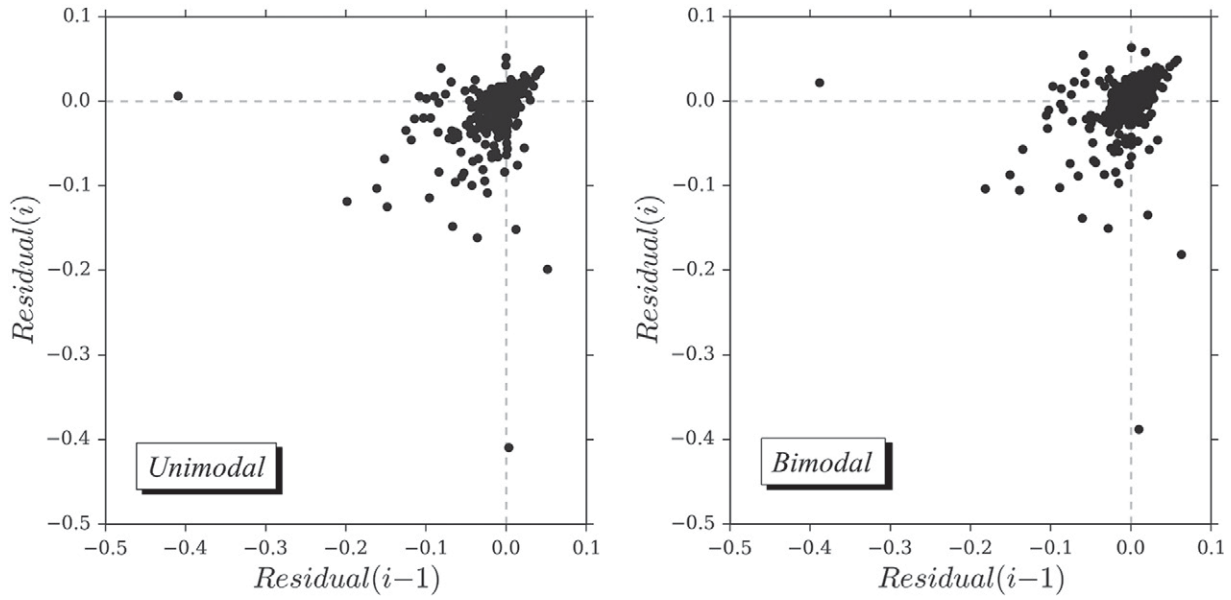

Fig. 8. A lag plot of the residuals between measured and simulated outflows. Results are for the HYDRUS model with the unimodal (left) and bimodal (right) functions of soil hydraulic properties.

of the model. Moreover, some uncertainty also arises from the evaluation of the soil depth in non-vegetated areas. Although an average depth of 4 cm was assumed, a slightly higher value may also be realistic considering the structure of the green roof (Fig. 1 and 4), and this would slightly modify the hydraulic response of the simulated green roof.

It can be concluded that HYDRUS, with both unimodal and bimodal functions of soil hydraulic properties, can accurately describe the hydraulic behavior of the considered green roof. The NSE indices are high, and residuals are randomly distributed for both models, with a slightly better performance with the bimodal functions. Because the bimodal model has proven to be more accurate in reproducing the real behavior of the green roof under small inflows, such as irrigation (Fig. 7), it was selected for further analysis.

Hydrological Analysis of the Green Roof

Cumulative inflow and outflow fluxes of the green roof are reported in Fig. 9. The green roof, coupled with the reuse system, was able to reduce the runoff volume by 25% during the considered period. Considering that the volume of water stored in the green roof substrate was only 16 mm (3% of the total inflow), evapotranspiration was the main factor in reducing the runoff volume. The steep gradients in cumulative outflow (Fig. 9) indicate that the green roof had a fast response to precipitation, with a negligible delay in the hydrograph. This aspect is directly related to the limited thickness of the green roof, which reduces the possible delay effect. On the other hand, cumulative outflow appeared flat when irrigation was applied. This behavior is particularly evident in September, when only negligible outflow fluxes were observed. At the beginning of October, cumulative outflow started to exhibit an increasing trend, caused by variations in actual evapotranspiration, as confirmed by the model. Figure 10 shows simulated actual root water uptake and evaporation from vegetated areas.

The first part of September (Fig. 10) was characterized by relatively high evapotranspiration, which lowered water contents in the soil substrate. As a consequence, only negligible outflow was produced by irrigation. The evapotranspiration rate dropped during the rain events between 9 and 11 Sept. 2015 due to the combined effects of high air humidity and low solar radiation.

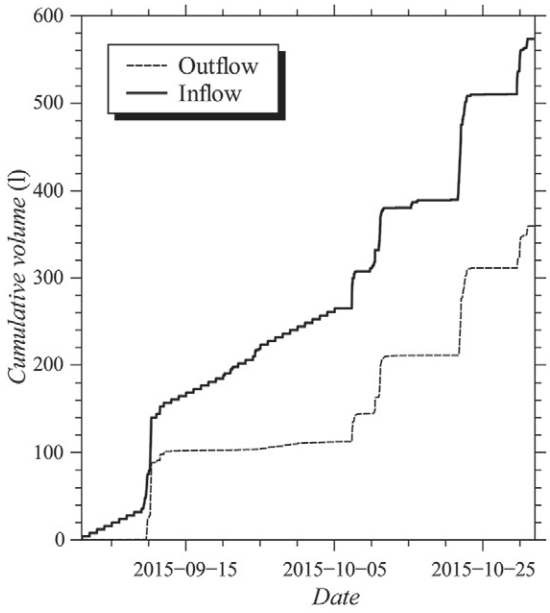

Fig. 9. A comparison between cumulative inflow and outflow from the green roof, simulated by HYDRUS-3D.

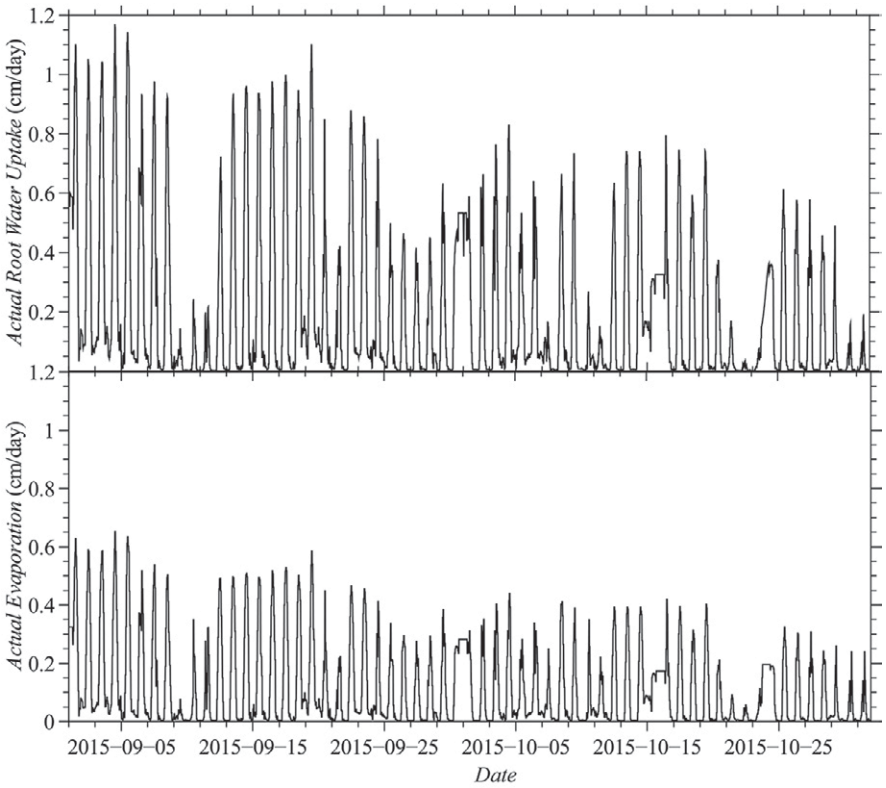

Fig. 10. Simulated actual root water uptake (top) and evaporation (bottom) from vegetated areas of the green roof.

At the end of September, due to the irrigation and lower evapotranspiration rates, the soil water contents were higher and actual transpiration lower. This behavior is shown in detail in Fig. 11. Between 25 and 30 Sept. 2015, the water content in vegetated areas ranged between 0.45 and 0.50, which corresponded to a pressure head range between −10 and −3 cm. In this pressure head range, plant transpiration is limited because of anaerobic conditions induced by high soil water contents (see the Feddes parameters in Table 3). Under these conditions, significant outflow was measured after irrigation (Fig. 3). This indicates that the model reproduced the dynamics of evapotranspiration in the green roof with good accuracy and that the parameters chosen for the water stress function are reasonable.

The comparison between pressure heads at the bottom of vegetated and non-vegetated areas of the green roof helps in identifying the different hydraulic responses of these two sections (Fig. 12). Before irrigation started, the bottom pressure head in the non-vegetated section was higher (in absolute value) than in the vegetated section. This indicates that the non-vegetated section dried out more and faster than the vegetated section due to its very low thickness. As irrigation started, the pressure head quickly increased in the non-vegetated section, reaching the seepage condition and producing outflow. On the other hand, in the vegetated section, the pressure head only approached the seepage condition without generating outflow. This indicates that only the non-vegetated section of the green roof was responsible for outflow after irrigation and that the irrigation system could be optimized to avoid the formation of outflow after irrigation.

Hydrological Performance during Precipitation Events

The hydrological response to single precipitation events is an important characteristic in the analysis of green roofs and LIDs in general. The measures such as peak flow reduction P_{red} (%), the peak flow delay t_{del} (min), and the volume reduction V_{red} (%) provide information about the hydrological benefits of the LID system to the urban drainage system. Four distinct rainfall events of a significant magnitude, one in September and three in October, were identified for further analysis of the hydrological performance of the green roof during single precipitation events. Figure 13 shows precipitation and measured and modeled outflow fluxes for each precipitation event, as well as the total volume of the entire precipitation event V_{prec} (mm) and measures P_{red} and V_{red}.

It is evident from Fig. 13 that the model exhibited good accuracy in reproducing the green roof hydraulic response also for single precipitation events. Modeled V_{red} and P_{red} are in agreement with information reported above. The model tended to overestimate the peak flow, especially for precipitation events characterized by an early peak (7 and 10 Oct. 2015), while the accuracy was very high for precipitation events with a delayed peak (9 Sept. and 21 Oct. 2015). Modeled volume reductions were sufficiently accurate. Only the analysis of the precipitation even on 21 October exhibited a significant deviation between the measured and modeled volume reductions.

The hydrological response of the green roof varied considerably for different precipitation events. Delay time t_{del} was on the order of

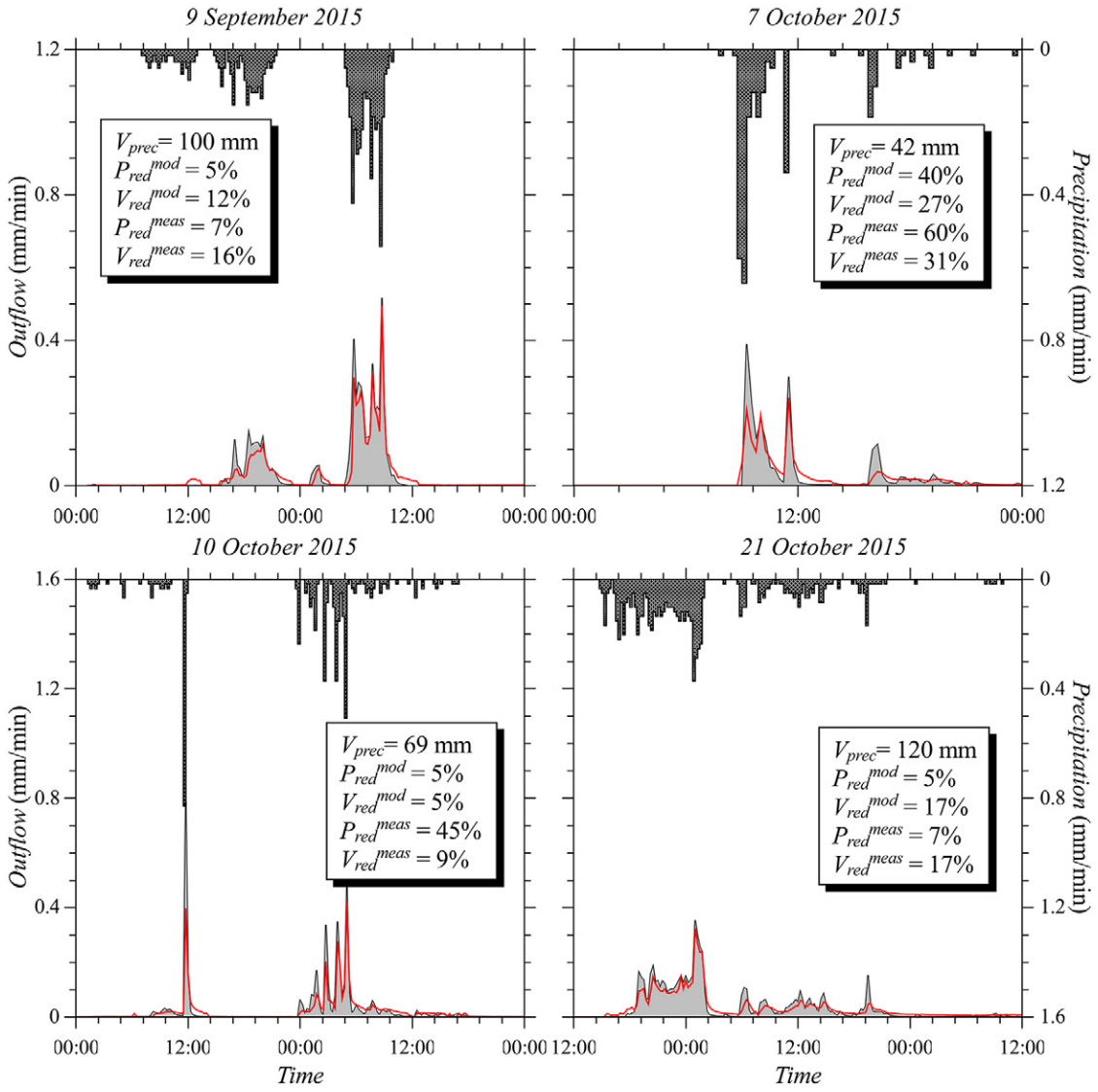

Fig. 11. Precipitation (dark area) and modeled (gray area) and measured (red line) outflow for four selected rainfall events in the analysis of the hydrological performance of the green roof during single precipitation events; P_{red}^{meas} and P_{red}^{mod} are the measured and modeled peak flow reductions, respectively, and V_{red}^{meas} and V_{red}^{mod} are the measured and modeled volume reductions, respectively.

15 min in all events, indicating that the delay effect was limited due to the limited thickness of the substrate. The largest P_{red} and V_{red} were observed for the event of 7 October. During this event, the precipitation peak occurred at the beginning of the event, which was preceded by more than 2 d of a dry period since irrigation was stopped on 5 October. Under these conditions, peak flow was partially attenuated by the relatively low initial water content of the soil substrate (Fig. 11). The effective volume reduction of the precipitation event (V_{eff}) was 13 mm.

Although the precipitation event of 10 October was also characterized by an early peak, the measured peak reduction of 45% was lower than that measured on 7 October. This can be attributed to the higher water content at the beginning of the event. While on 7 October the initial water content was about 0.32, it was about 0.39 on 10 October. The higher water content on 10 October resulted in a lower attenuation capacity of the substrate. For the events of 9 and 21 September, P_{red} was only 7%. For both events, peak flow was preceded by low-intensity precipitation, which increased the soil water content and, as a consequence, lowered the capacity of the green roof to attenuate the peak of precipitation. The effective volume reduction (V_{eff}) for the event of 21 October was 20.4 mm, which was the highest among all of the evaluated precipitation events. Before this event started, the water content of the substrate reached the lowest value of 0.2, significantly increasing the soil storage capacity.

It can be concluded that the green roof response to precipitation, during the analyzed period, was influenced primarily by the antecedent substrate moisture and secondarily by the precipitation pattern. Positively skewed and leptokurtic precipitation distributions tended to exhibit the largest peak flow reduction, while

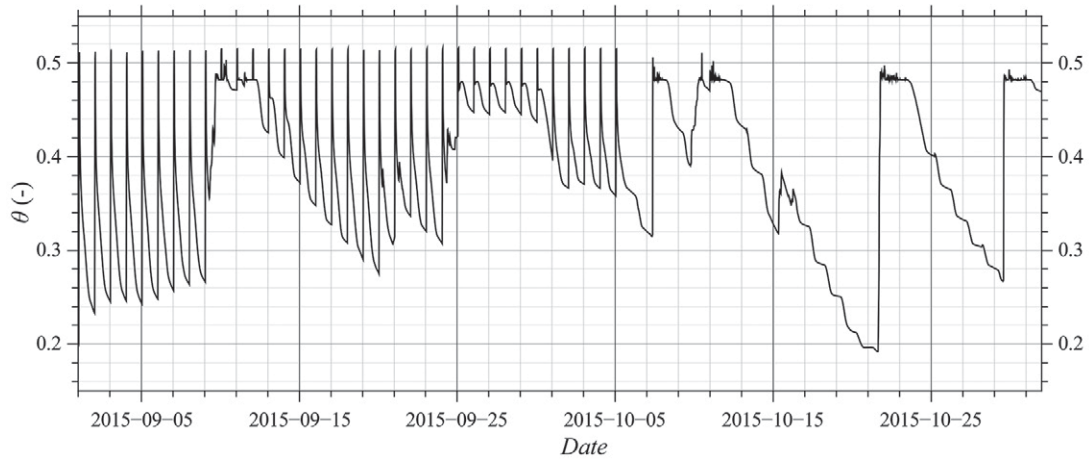

Fig. 12. Simulated water contents (θ) in the vegetated section of the green roof at a depth of 4 cm.

negatively skewed and platykurtic precipitation distributions were likely to have lower peak reductions. The volume retained by the green roof was mainly determined by the initial substrate moisture and was independent of the precipitation pattern. It must be emphasized that these conclusions are not general but are restricted to the specific investigated green roof. The validated model could be used in a sensitivity analysis, in which, together with other factors (e.g., substrate moisture, slope, substrate depth, etc.), the effect of the precipitation pattern on the green roof response can be investigated using synthetically designed storms (Carbone et al., 2015b).

Conclusions

The goal of this study was to provide a comprehensive numerical analysis of the hydrological behavior of a green roof. The widely used mechanistic model HYDRUS-3D was used to model the hydrological responses to precipitation, evapotranspiration, and irrigation fluxes of green roof installed at the University of Calabria. The green roof was characterized by a high degree of complexity; it included different soil depths, vegetated and non-vegetated areas, and non-uniformity in the boundary conditions.

Moreover, considering the lack of studies with regard to the unsaturated hydraulic properties of soil substrates in green roofs, the simplified evaporation method was used to determine both the soil water retention curve and the unsaturated hydraulic conductivity function of the soil used in the green roof. The soil exhibited a bimodal pore structure, characterized by a weakly pronounced secondary pore system and a high hydraulic conductivity. The bimodal functions proposed by Durner (1994) best represented the hydraulic properties of the substrate. The unimodal VGM relationships were also tested, but their description of unsaturated hydraulic properties was less accurate, especially for the unsaturated hydraulic conductivity.

Soil hydraulic parameters obtained from the evaporation method were then used in HYDRUS-3D to model the hydrological behavior of the green roof during a 2-mo time period. Both the unimodal and bimodal functions of soil hydraulic properties

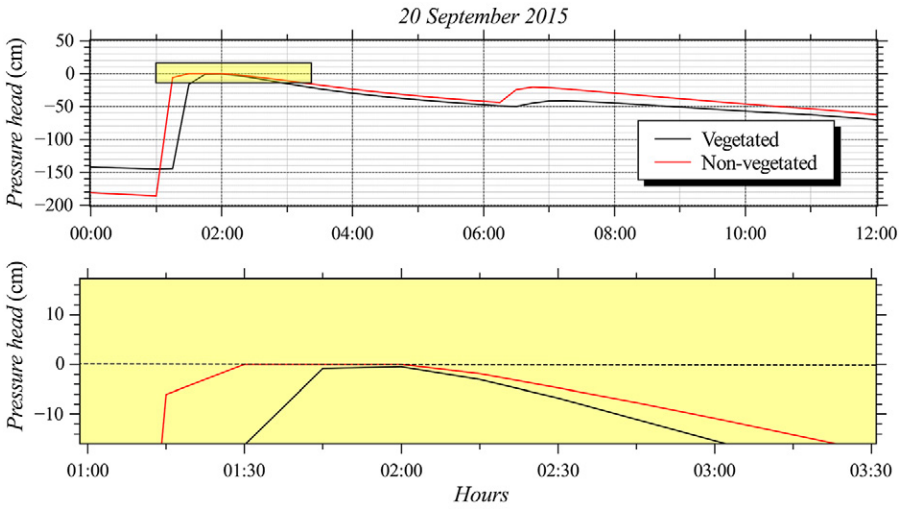

Fig. 13. Pressure heads at the bottom of the vegetated (black) and non-vegetated (red) sections of the green roof simulated by HYDRUS-3D. The yellow rectangular area in the top figure is expanded in the bottom figure. The dashed line represents a seepage condition.

were used in the analysis. The numerical simulation considered precipitation, evaporation, root water uptake, and irrigation. The Feddes model was used to represent the water stress response function of plants installed on the green roof. Feddes' parameters were adjusted by taking into account the behavior of succulent plants such as *Carpobrotus edulis* under different soil water content regimes. The NSE index was used to compare the simulated and measured outflows. The NSE indices were 0.74 and 0.8 for the model predictions with the unimodal and bimodal functions, respectively, indicating a good accuracy. Both models slightly overestimated some outflow fluxes. The randomness of the residuals was confirmed by the absence of evident patterns in the lag plot. The main difference between the two models was in the description of the hydraulic behavior of the green roof after irrigation. While the unimodal model failed to reproduce small measured outflows, the bimodal model gave a more accurate description. This further confirmed the accuracy of this model. The validated model with bimodal functions was used to analyze the hydrological performance of the green roof during the entire simulation period and to investigate its hydrological response to single precipitation events. About 25% of the total inflow volume was returned to the atmosphere by evaporation and transpiration. The analysis of simulated pressure heads revealed that the non-vegetated section of the green roof was responsible for the small outflow fluxes following irrigation. This suggests that the irrigation system could be further optimized. The analysis of the hydrological response of the green roof to single precipitation events highlighted the importance of the initial soil moisture for volume and peak flow reductions. Furthermore, the analysis revealed that positively skewed and leptokurtic precipitation distributions are likely to exhibit the largest peak flow reductions. The volume reduction is mainly influenced by the initial soil moisture and is insensitive to the precipitation pattern.

The performance of the model can be improved by a better description of the soil hydraulic properties, especially near saturation, considering that during intense precipitation events, significant portions of the domain become saturated. Moreover, uncertainties in rainfall measurements and in geometric characteristics of the green roof can introduce a further bias to the simulated results. A sensitivity analysis followed by an uncertainty analysis can help in identifying the most sensitive parameters and address the source of uncertainty (e.g., Brunetti et al., 2016). Nevertheless, it can be concluded that the use of measured soil hydraulic properties with a mechanistic model can be a valuable tool for the analysis of green roofs and other LIDs and can boost the widespread adoption of such systems as a viable alternative to traditional urban drainage systems.

Acknowledgments

The study was co-funded by the Italian National Operative Project (PON)–Research and Competitiveness for the convergence regions 2007/2013-I Axis "Support to structural changes," Operative Objective 4.1.1.1 "Scientific-technological generators of transformation processes of the productive system and creation of new sectors," Action II: "Interventions to support industrial research."

References

Allen, R.G., L.S. Pereira, D. Raes, and M. Smith. 1998. Crop evapotranspiration. Irrig. Drain. Pap. 56. FAO, Rome.

Arya, L.M. 2002. Simultaneous determination of water transmission and retention properties: Wind and hot-air methods. In: J.H. Dane and G.C. Topp, editors, Methods of soil analysis. Part 4. Physical methods. SSSA Book Ser. 5. SSSA, Madison, WI. p. 916–926. doi:10.2136/sssabookser5.4.c38

Bengtsson, L., L. Grahn, and J. Olsson. 2004. Hydrological function of a thin extensive green roof in southern Sweden. Nord. Hydrol. 36:259–268.

Blanusa, T., M.M. Vaz Monteiro, F. Fantozzi, E. Vysini, Y. Li, and R.W.F. Cameron. 2013. Alternatives to *Sedum* on green roofs: Can broad leaf perennial plants offer better "cooling service"? Build. Environ. 59:99–106. doi:10.1016/j.buildenv.2012.08.011

Brattebo, B.O., and D.B. Booth. 2003. Long-term stormwater quantity and quality performance of permeable pavement systems. Water Res. 37:4369–4376. doi:10.1016/S0043-1354(03)00410-X

Brunetti, G., J. Šimůnek, and P. Piro. 2016. A comprehensive numerical analysis of the hydraulic behavior of permeable pavement. J. Hydrol. 540:1146–1161. doi:10.1016/j.jhydrol.2016.07.030

Carbone, M., G. Brunetti, and P. Piro. 2014. Hydrological performance of a permeable pavement in Mediterranean climate. In: 14th SGEM GeoConference on Water Resources: Forest, Marine and Ocean Ecosystems, Albena, Bulgaria. 17–26 June 2014. Book 3. Vol. 1. Int. Multidiscip. Sci. GeoConf., Sofia, Bulgaria. p. 381–388. doi:10.5593/SGEM2014/B31/S12.050.

Carbone, M., G. Brunetti, and P. Piro. 2015a. Modelling the hydraulic behaviour of growing media with the explicit finite volume solution. Water 7:568–591. doi:10.3390/w7020568

Carbone, M., M. Turco, G. Brunetti, and P. Piro. 2015b. A cumulative rainfall function for subhourly design storm in Mediterranean urban areas. Adv. Meteorol. 2015:1–10. doi:10.1155/2015/528564

Coffman, L.S. 2002. Low-impact development: An alternative stormwater management technology. In: R.L. France, editor, Handbook of water sensitive planning and design. Lewis Publ., Boca Raton, FL. p. 97–123.

Collins, K.A., W.F. Hunt, and J.M. Hathaway. 2008. Hydrologic comparison of four types of permeable pavement and standard asphalt in eastern North Carolina. J. Hydrol. Eng. 13:1146–1157. doi:10.1061/(ASCE)1084-0699(2008)13:12(1146)

Dane, J.H., and J.W. Hopmans. 2002. Water retention and storage: Pressure plate extractor. In: J.H. Dane and G.C. Topp, editors, Methods of soil analysis. Part 4. Physical methods. SSSA Book Ser. 5. SSSA, Madison, WI. p. 688–690. doi:10.2136/sssabookser5.4.c25

Davis, A.P. 2008. Field performance of bioretention: Hydrology impacts. J. Hydrol. Eng. 13:90–95. doi:10.1061/(ASCE)1084-0699(2008)13:2(90)

Duan, Q., S. Sorooshian, and V. Gupta. 1992. Effective and efficient global optimization for conceptual rainfall–runoff models. Water Resour. Res. 28:1015–1031. doi:10.1029/91WR02985

Durhman, A.K., D.B. Rowe, and C.L. Rugh. 2006. Effect of watering regimen on chlorophyll fluorescence and growth of selected green roof plant taxa. HortScience 41:1623–1628.

Durner, W. 1994. Hydraulic conductivity estimation for soils with heterogeneous pore structure. Water Resour. Res. 30:211–223. doi:10.1029/93WR02676

Elliott, A., and S. Trowsdale. 2007. A review of models for low impact urban stormwater drainage. Environ. Modell. Softw. 22:394–405. doi:10.1016/j.envsoft.2005.12.005

Feddes, R.A., P.J. Kowalik, and H. Zaradny. 1978. Simulation of field water use and crop yield. PUDOC, Wageningen, the Netherlands.

Getter, K.L., D.B. Rowe, and J.A. Andresen. 2007. Quantifying the effect of slope on extensive green roof stormwater retention. Ecol. Eng. 31:225–231. doi:10.1016/j.ecoleng.2007.06.004

Hanscom, Z., and I.P. Ting. 1978. Responses of succulents to plant water stress. Plant Physiol. 61:327–330. doi:10.1104/pp.61.3.327

Hilten, R.N., T.M. Lawrence, and E.W. Tollner. 2008. Modeling stormwater runoff from green roofs with HYDRUS-1D. J. Hydrol. 358:288–293. doi:10.1016/j.jhydrol.2008.06.010

Hu, S. 1987. Book review: Akaike information criterion statistics. Math. Comput. Simul. 29:452. doi:10.1016/0378-4754(87)90094-2

Kasmin, H., V.R. Stovin, and E.A. Hathway. 2010. Towards a generic rainfall–runoff model for green roofs. Water Sci. Technol. 62:898–905. doi:10.2166/wst.2010.352

Klute, A., and C. Dirksen. 1986. Hydraulic conductivity and diffusivity. Laboratory methods. In: Methods of soil analysis. Part 1. Physical and mineralogical methods. 2nd ed. SSSA Book Ser. 5. SSSA and ASA, Madison, WI. p. 687–734. doi:10.2136/sssabookser5.1.2ed.c28

Kundzewicz, Z., M. Radziejewski, and I. Pínskwar. 2006. Precipitation extremes in the changing climate of Europe. Clim. Res. 31:51–58. doi:10.3354/cr031051

Lazzarin, R.M., F. Castellotti, and F. Busato. 2005. Experimental measurements and numerical modelling of a green roof. Energy Build. 37:1260–1267. doi:10.1016/j.enbuild.2005.02.001

Li, Y., and R.W. Babcock. 2014. Green roof hydrologic performance and modeling: A review. Water Sci. Technol. 69:727–738. doi:10.2166/wst.2013.770

Li, Y., and R.W. Babcock. 2015. Modeling hydrologic performance of a green roof system with HYDRUS-2D. J. Environ. Eng. 141:04015036. doi:10.1061/(ASCE)EE.1943-7870.0000976

Locatelli, L., O. Mark, P.S. Mikkelsen, K. Arnbjerg-Nielsen, M.B. Jensen, and P.J. Binning. 2014. Modelling of green roof hydrological performance for urban drainage applications. J. Hydrol. 519:3237–3248. doi:10.1016/j.jhydrol.2014.10.030

Metselaar, K. 2012. Water retention and evapotranspiration of green roofs and possible natural vegetation types. Resour. Conserv. Recycl. 64:49–55. doi:10.1016/j.resconrec.2011.12.009

Min, S.-K., X. Zhang, F.W. Zwiers, and G.C. Hegerl. 2011. Human contribution to more-intense precipitation extremes. Nature 470:378–381. doi:10.1038/nature09763

Moriasi, D.N., J.G. Arnold, M.W. Van Liew, R.L. Binger, R.D. Harmel, and T.L. Veith. 2007. Model evaluation guidelines for systematic quantification of accuracy in watershed simulations. Trans. ASABE 50:885–900. doi:10.13031/2013.23153

Nash, J.E., and J.V. Sutcliffe. 1970. River flow forecasting through conceptual models: I. A discussion of principles. J. Hydrol. 10:282–290. doi:10.1016/0022-1694(70)90255-6

Pertassek, T., A. Peters, and W. Durner. 2015. HYPROP-FIT software user's manual, Version 3.0. UMS GmbH, Munich, Germany.

Peters, A., and W. Durner. 2006. Improved estimation of soil water retention characteristics from hydrostatic column experiments. Water Resour. Res. 42:W11401. doi:10.1029/2006WR004952

Peters, A., and W. Durner. 2008. Simplified evaporation method for determining soil hydraulic properties. J. Hydrol. 356:147–162. doi:10.1016/j.jhydrol.2008.04.016

Ritchie, J.T. 1972. Model for predicting evaporation from a row crop with incomplete cover. Water Resour. Res. 8:1204–1213. doi:10.1029/WR008i005p01204

Rosenberg, N.J., L.B. Blaine, and B.V. Shashi. 1983. Microclimate: The biological environment. John Wiley & Sons, New York.

Sayed, O.H. 2001. Crassulacean acid metabolism 1975–2000, a check list. Photosynthetica 39:339–352. doi:10.1023/A:1020292623960

Schaap, M.G., and F.J. Leij. 2000. Improved prediction of unsaturated hydraulic conductivity with the Mualem–van Genuchten model. Soil Sci. Soc. Am. J. 64:843–851. doi:10.2136/sssaj2000.643843x

Schaap, M.G., F.J. Leij, and M.Th. van Genuchten. 2001. Rosetta: A computer program for estimating soil hydraulic parameters with hierarchical pedotransfer functions. J. Hydrol. 251:163–176. doi:10.1016/S0022-1694(01)00466-8

Schindler, U., 1980. Ein Schnellverfahren zur Messung der Wasserleitfähigkeit im teilgesättigten Boden an Stechzylinderproben. Arch. Acker-Pflanzenbau Bodenkd. 24:1–7.

Schindler, U., W. Durner, G. von Unold, L. Mueller, and R. Wieland. 2010a. The evaporation method: Extending the measurement range of soil hydraulic properties using the air-entry pressure of the ceramic cup. J. Plant Nutr. Soil Sci. 173:563–572. doi:10.1002/jpln.200900201

Schindler, U., W. Durner, G. von Unold, and L. Müller. 2010b. Evaporation method for measuring unsaturated hydraulic properties of soils: Extending the measurement range. Soil Sci. Soc. Am. J. 74:1071–1083. doi:10.2136/sssaj2008.0358

Servat, E., and A. Dezetter. 1991. Selection of calibration objective functions in the context of rainfall–runoff modelling in a Sudanese savannah area. Hydrol. Sci. J. 36:307–330. doi:10.1080/02626669109492517

She, N., and J. Pang. 2010. Physically based green roof model. J. Hydrol. Eng. 15:458–464. doi:10.1061/(ASCE)HE.1943-5584.0000138

Šimůnek, J., M.Th. van Genuchten, and M. Šejna. 2008. Development and applications of the HYDRUS and STANMOD software packages and related codes. Vadose Zone J. 7:587–600. doi:10.2136/vzj2007.0077

Šimůnek, J., M.Th. van Genuchten, and O. Wendroth. 1998. Parameter estimation analysis of the evaporation method for determining soil hydraulic properties. Soil Sci. Soc. Am. J. 62:894–905. doi:10.2136/sssaj1998.03615995006200040007x

Starry, O., J.D. Lea-Cox, J. Kim, and M.W. van Iersel. 2014. Photosynthesis and water use by two *Sedum* species in green roof substrate. Environ. Exp. Bot. 107:105–112. doi:10.1016/j.envexpbot.2014.05.014

Sutanto, S.J., J. Wenninger, A.M.J. Coenders-Gerrits, and S. Uhlenbrook. 2012. Partitioning of evaporation into transpiration, soil evaporation and interception: A comparison between isotope measurements and a HYDRUS-1D model. Hydrol. Earth Syst. Sci. 16:2605–2616. doi:10.5194/hess-16-2605-2012

Taylor, S.A., and G.L. Ashcroft. 1972. Physical edaphology: The physics of irrigated and nonirrigated soils. W.H. Freeman, San Francisco.

Torres, E.A., and A. Calera. 2010. Bare soil evaporation under high evaporation demand: A proposed modification to the FAO-56 model. Hydrol. Sci. J. 55:303–315. doi:10.1080/02626661003683249

UMS GmbH. 2015. Manual HYPROP, Version 2015-01. UMS GmbH, Munich, Germany.

van Dam, J.C., P. Groenendijk, R.F.A. Hendriks, and J.G. Kroes. 2008. Advances of modeling water flow in variably saturated soils with SWAP. Vadose Zone J. 7:640–653. doi:10.2136/vzj2007.0060

van Genuchten, M.Th. 1980. A closed-form equation for predicting the hydraulic conductivity of unsaturated soils. Soil Sci. Soc. Am. J. 44:892–898. doi:10.2136/sssaj1980.03615995004400050002x

Vesuviano, G., F. Sonnenwald, and V. Stovin. 2014. A two-stage storage routing model for green roof runoff detention. Water Sci. Technol. 69:1191–1197. doi:10.2166/wst.2013.808

Wendroth, O., W. Ehlers, H. Kage, J.W. Hopmans, J. Halbertsma, and J.H.M. Wösten. 1993. Reevaluation of the evaporation method for determining hydraulic functions in unsaturated soils. Soil Sci. Soc. Am. J. 57:1436–1443. doi:10.2136/sssaj1993.03615995005700060007x

Wesseling, J., J. Elbers, P. Kabat, and B. Van den Broek. 1991. SWATRE: Instructions for input. Winand Staring Ctr., Wageningen, the Netherlands.

Zhang, S.H., and Y.P. Guo. 2013. Analytical probabilistic model for evaluating the hydrologic performance of green roofs. J. Hydrol. Eng. 18:19–28. doi:10.1061/(ASCE)HE.1943-5584.0000593